Grid following converters stability study and control enhancements using an improved test setup

Lamrani, Yahya; Huang, Liang; Colas, Frédéric; Guillaud, Xavier; Blaajberg, Frede; Cardozo, Carmen; Prevost, Thibault

Published in:
IET Conference Proceedings

DOI (link to publication from Publisher):
10.1049/icp.2023.1309

Publication date:
2023

Document Version
Early version, also known as pre-print

Grid following converters stability study and control enhancements using an improved test setup

SUBMISSION DATE / POSTED DATE

23-02-2023 / 06-03-2023

CITATION

Lamrani, Yahya; Huang, Liang; Colas, Frédéric; Guillaud, Xavier; Blaabjerg, Frede; Cardozo, Carmen; et al. (2023): Grid following converters stability study and control enhancements using an improved test setup. TechRxiv. Preprint. https://doi.org/10.36227/techrxiv.22146776.v2

DOI

10.36227/techrxiv.22146776.v2

Grid following converters stability study and control enhancements using an improved test setup

Yahya Lamrani[1, 3], Liang Huang[5], Frédéric Colas[1, 2], Xavier Guillaud[1, 3], Frede Blaajberg[5], Carmen Cardozo[6], Thibault Prevost[6]*

[1]*Univ. Lille, ULR 2697 - L2EP, F-59000 Lille, France*
[2]*Arts et Metiers Institute of Technology, F-59000 Lille, France*
[3]*Centrale Lille, F-59000 Lille, France*
[4]*Junia, F-59000 Lille, France*
[5]*Department of Energy Technology, Aalborg University, Aalborg, Denmark*
[6]*RTE R&D, 92919 La Défense, France*
**yahyalamrani@centralelille.fr*

Keywords: Grid following control, Small-signal stability, Interaction phenomena

Abstract

To insure a stable and reliable operation of the existing and future grids, it is important to study the stability of the power electronic based converters' controls which can replace synchronous generation. Most existing studies use a Thévenin equivalent model of the grid to test the grid following controls. The present article demonstrates the limits of these studies. An alternative setup is proposed and is shown to provide more insight into the underlying mechanisms of the grid following control behaviour in weak grids, using a linearized state space model. These insights are exploited to propose further improvements to the control. These improvements are shown to extend the stability of the control while reducing the interactions among converters.

1 Introduction

As the European Union ramps up its renewable energy production to meet the Green Deal objectives, the power systems are experiencing new challenges to remain stable [1]. The stability has been traditionally guaranteed by the synchronous generators, but as non-synchronous renewable generation replaces this synchronous generation, the stability of power systems needs to be vigilantly studied under these new conditions. The consensus regarding this trend is that it destabilizes the power system [2]. The most commonly used power electronics interfaced generation are controlled using grid following (GFL) controls. The GFL sensitivity to the grid's strength is a well-documented issue in the literature as many articles have studied the behaviour of GFL converters in varying grid strengths and reported their small signal instability under weak grid conditions [3], [4]. Later studies have provided guidelines to tune GFL controls for better small signal stability under weak grid conditions [5]–[7].

The methodologies most commonly used for this type of study consist of a Thévenin equivalent setup, with the grid's impedance chosen to reflect a short-circuit ratio (SCR) value representing a set grid's strength. This setup is then modelled using a small-signal linearized model based on state-space or impedance representations to better understand the underlying stability issues [8].

However, this setup does not really reflect the real use case of GFL controls. The SCR has been reported to fail as a metric for networks with a high penetration rate of converters [9]. A weak grid is often correlated with long-distance transmission and the presence of nearby non-synchronous generations [2]. Such instability sources are not duplicated by the common Thévenin equivalent studies. The Thévenin equivalent also fails to study interaction phenomena among GFL converters. Such interactions have been reported, while using simplified models only, to cause instability [10], [11].

The present article presents a formal demonstration of the limits of Thévenin equivalent small-signal stability studies for proper tuning of GFL controls. As an alternative, it proposes a test setup to further improve the small-signal stability of the GFL controls in a use case that is more realistic by overcoming the limits of the Thévenin equivalent limits and by accounting for interaction phenomena.

The rest of the paper is organized as follows: Section 2 presents the Thévenin equivalent setup and the generic GFL control structure. Using the existing literature's recommendations, it can be shown the limits of the Thevenin equivalent study originate from the static power transfer limit rather than the control of the converter. Section 3 introduces the proposed test setup; it is shown the stability limit is no longer restrained by the static limit. A state-space linearized model is built to study interaction phenomena and the system's sensitivity to the grid strength. Section 4 exploits the findings to propose further improvements to the GFL controls and verifies the improvements using a state-space linearized model.

2 Small signal stability analysis on a Thevenin equivalent

In this section, the Thévenin equivalent setup is described and the static limit of the setup is calculated. A generic GFL control structure is then presented and tuned using the literature's recommendations [5], [12]. The state-space linearized model of the GFL control in the Thévenin equivalent setup is developed and studied to showcase that the GFL control remains stable up to the static limit. Finally, findings are validated and confirmed by simulations.

2.1 System description

The test setup is shown in figure 1, the voltage source converter (VSC) converter is connected to the grid modelled by a Thévenin equivalent. The converter is connected via a step-up transformer modelled here by an RL impedance (in the p.u model), and the grid impedance is chosen to reflect the SCR at the Point of common coupling (PCC). The converter and the circuit parameters are chosen to represent a real use case of a VSC connected to the transmission grid [13]. The parameters and the base values for the p.u model are detailed in table 1.

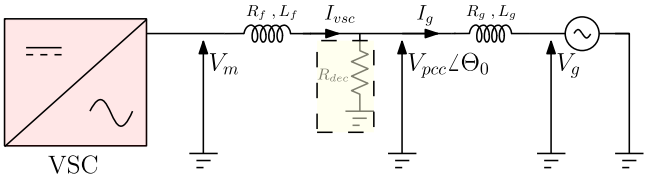

Fig. 1 Thévenin equivalent Setup

The static limit of the described setup is defined at the operating point corresponding to the VSC's nominal power injection at the nominal voltage at the lowest SCR while respecting the reactive power limits.

A simple load flow calculation can show that:

$$\begin{cases} SCR = 1.74 \\ P_{VSC} = P_{nom} = 0.958\, p.u \Longrightarrow Q = Q_{max} = 0.287\, p.u \\ U_{VSC} = U_{nom} = 1\, p.u \end{cases} \quad (1)$$

Therefore, the operating point described by (1) is considered the static limit of the Thévenin equivalent setup.

Table 1 VSC and grid parameters

Parameter	Symbol	Value
Base Power	S_b	1044 MVA
Base Voltage	U_b	400 kV
Base frequency	ω_b	314 rad/s
VSC apparent power	S_{VSC}	1044 MVA
VSC nominal power	P_{nom}	1 GW
VSC nominal voltage	U_{nom}	400 kV
VSC maximum reactive power	Q_{max}	300 MVAr
VSC Transformer's Leakage inductance	L_f	0.15 p.u
VSC Transformer's resistor	R_f	0.005 p.u
Grid's inductance	L_g	$1/SCR$
Grid's resistance	R_g	0 p.u

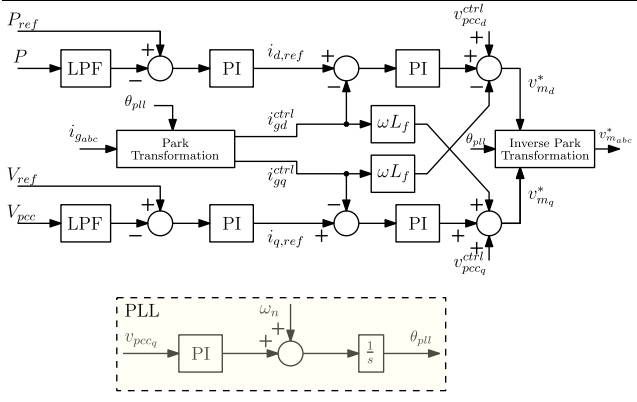

Fig. 2 GFL control structure

2.2 GFL control

The VSC under study is controlled using a generic vector-controlled, Phase-Locked Loop (PLL) synchronized GFL control [14]. This converter is controlled to track the active power injection to P_{ref} and to regulate the PCC's voltage at V_{ref}. The control structure is illustrated in figure 2.

Using various design studies and recommendations for GFL control under weak grid conditions, the present GFL control is tuned as shown in table 2 [5], [6], [15].

Table 2 VSC control parameters

Control	Parameter	Value
Input filters	$\omega^{inputs}_{LPF,-3dB}$	5000 rad/s
Outer loops tuning	$\omega_{P,-3dB}$	10 rad/s
	$\omega_{V,-3dB}$	50 rad/s
	$\omega^{outer\ loops}_{LPF,-3dB}$	300 rad/s
PLL	ω_n	50 rad/s
	ξ	1
Current loops tuning	$\omega_{cc,-3dB}$	4000 rad/s
	Modulus optimum tuning	

2.2 System and Control equations

The linearized small-signal models are derived from the time-domain equations describing the test setup behaviour in the synchronous dq-frame. A parasitic shunt resistor R_{dec} is added at the PCC to decouple the converter side and the grid side. The active power leakage through the parasitic shunt resistor is under 1% of the rated active power. Simulating the setup with and without the decoupling resistor shows that the system displays the same dynamic behaviour.

2.2.1 Time-domain equations

The circuit equations (in p.u) are split thanks to R_{dec} :

$$\begin{cases} \frac{d\, i^d_{vsc}}{dt} = \frac{\omega_b}{L_f}\left(v^d_m - v^d_{pcc} - R_f i^d_{vsc} + \omega L_f i^q_{vsc}\right) \\ \frac{d\, i^q_{vsc}}{dt} = \frac{\omega_b}{L_f}\left(v^q_m - v^q_{pcc} - R_f i^q_{vsc} - \omega L_f i^d_{vsc}\right) \end{cases} \quad (2)$$

$$\begin{cases} \frac{d\, i^d_g}{dt} = \frac{\omega_b}{L_f}\left(v^d_{pcc} - v^d_g + \omega L_f i^q_g\right) \\ \frac{d\, i^q_g}{dt} = \frac{\omega_b}{L_f}\left(v^q_{pcc} - v^q_g - \omega L_f i^d_g\right) \end{cases} \quad (3)$$

$$v^{dq}_{pcc} = R_{dec}\left(i^{dq}_{vsc} - i^{dq}_g\right) \quad (4)$$

The control equations can be derived from the control blocks shown in figure 2. These equations are described in the control reference frame denoted by the superscript "ctrl", the inputs and outputs are rotated using the Park and inverse Park transformation:

$$\begin{cases} \begin{bmatrix} v^{d,ctrl}_{pcc} \\ v^{q,ctrl}_{pcc} \end{bmatrix} = \begin{bmatrix} \cos(\theta_{pll} - \theta_0) & \sin(\theta_{pll} - \theta_0) \\ -\sin(\theta_{pll} - \theta_0) & \cos(\theta_{pll} - \theta_0) \end{bmatrix} \begin{bmatrix} v^d_{pcc} \\ v^q_{pcc} \end{bmatrix} \\ \begin{bmatrix} i^{d,ctrl}_{vsc} \\ i^{q,ctrl}_{vsc} \end{bmatrix} = \begin{bmatrix} \cos(\theta_{pll} - \theta_0) & \sin(\theta_{pll} - \theta_0) \\ -\sin(\theta_{pll} - \theta_0) & \cos(\theta_{pll} - \theta_0) \end{bmatrix} \begin{bmatrix} i^d_{vsc} \\ i^q_{vsc} \end{bmatrix} \\ \begin{bmatrix} v^d_m \\ v^q_m \end{bmatrix} = \begin{bmatrix} \cos(\theta_{pll} - \theta_0) & -\sin(\theta_{pll} - \theta_0) \\ \sin(\theta_{pll} - \theta_0) & \cos(\theta_{pll} - \theta_0) \end{bmatrix} \begin{bmatrix} v^{d,ctrl}_m \\ v^{q,ctrl}_m \end{bmatrix} \end{cases} \quad (5)$$

2.2.2 Linearized state-space model

The equations derived from the control structure and the circuit are used to build the linearized state-space model:

$$\begin{cases}\Delta\dot{x} = A\Delta x + B\Delta u \\ \Delta y = C\Delta x + D\Delta u\end{cases} \quad (6)$$

With the state variables being:

$$x = (i_g^{dq}, i_{vsc}^{dq}, v_{pcc}^{dq,filt}, i_{vsc}^{dq,filt}, P^{filt}, V_{pcc}^{filt}, \zeta^P, \zeta^V, \zeta^{i_d}, \zeta^{i_q}, \zeta^{PLL}, \theta^{PLL}) = (i_g^{dq}, x^{VSC}) \quad (7)$$

Where ζ represents the state variables associated with input of the PI controllers' integrators.

The stability of the system is deduced from the analysis of the eigenvalues of the matrix A. Following the evolution of these eigenvalues when varying a circuit or control parameter provides insight into the system's sensitivity to a specific parameter. Analysing the participation factors of the poorly damped and potentially unstable eigenvalues can identify the state variables most contributing to the eigenvalue and hint at the potential improvement paths to explore.

Figure 3(a) shows the eigenvalues of the system at the static limit. Since all eigenvalues have a negative real part, it can be deduced that the GFL control remains stable up to the static limit. This conclusion is confirmed by simulation, shown in figure 3(b), where a $\frac{\pi}{40}$ phase jump is applied to the system. The phase jump event type provides better insight into the modes of the system as it directly disturbs the control inner loops (unlike a P_{ref} change for example) and does not alter the operating point around which the model has been linearized.

As the figure shows, the system regains its stable operating point. Furthermore, the fast oscillations and the response time are identical to the modes identified by the eigenvalues.

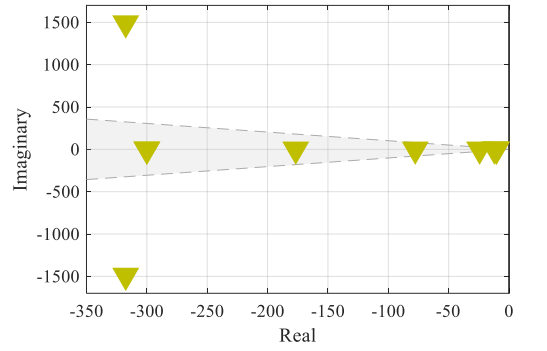

(a)

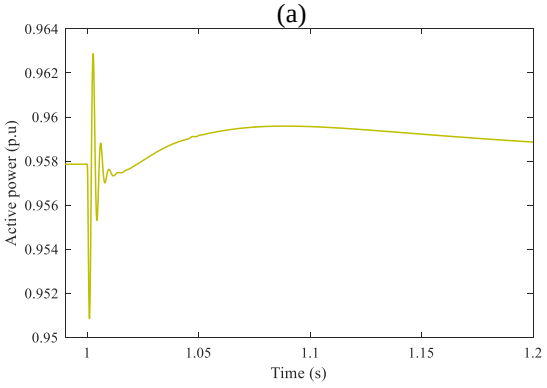

(b)

Fig. 3 (a) Eigenvalues of the linearized model, (b) Time-domain simulation of the non-linear model

3 Proposed setup: 2 converters test case

As previously demonstrated, the Thévenin equivalent study is only limited by the static limit of the setup when the GFL is properly tuned. Moreover, it is impossible to highlight the reported interaction phenomena in this setup.

In order to overcome both limitations, the setup shown in figure 4 is proposed. Here, the system under study consists of two converters with the power flowing from VSC1 to VSC2. With no power flowing through the grid's impedance, its value can be further increased without reaching the reactive power limits of the converters, thus representing a situation of a remote non-meshed connection to the transmission grid. Additionally, this setup allows highlighting potential interaction phenomena.

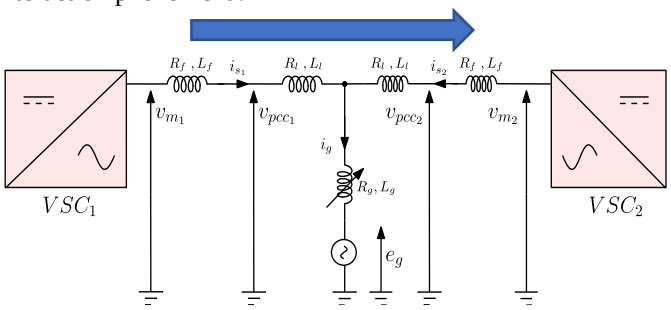

Fig. 4 Proposed setup

The base values, the VSC control and parameters R_l, L_l represent the typical values of a 400kV 30 km long overhead line (OHL). The new parameters are given in the table 3:

Table 3 modified parameters of the setup

Parameter	Symbol	Value
OHL inductance	L_l	0.144 p.u
OHL resistance	R_l	0.0072 p.u
Grid's inductance	L_g	0.95 p.u
Grid's resistance	R_g	0 p.u

In coherence with the logic of the previous section, the operating point is chosen to reflect a nominal power injection at the nominal voltage:

$$\begin{cases} P_{ref,VSC1} = -P_{ref,VSC2} = 0{,}958\ p.u \\ V_{pcc,ref,VSC1} = V_{pcc,ref,VSC2} = e_g = 1\ p.u \end{cases} \quad (8)$$

3.1 Validation of the linearized model

The linearized state-space model of the proposed setup is built and validated for the nominal operating point as shown in figure 5. The event used for the validation is a $\frac{\pi}{40}$ phase jump applied at e_g.

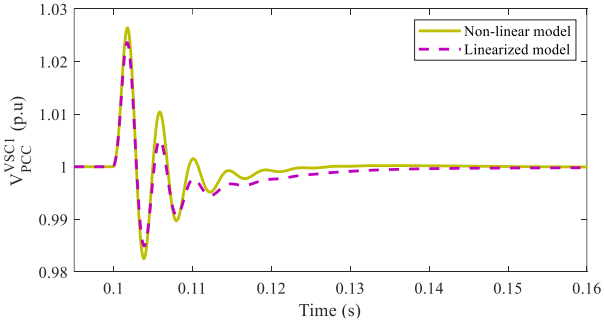

Fig. 5 Time-domain validation of the linearized model

It can be seen that the linearized model reflects the same dynamic behaviour of the non-linear model (modes' frequencies and settling time). A slight difference is however observed for the damping of the system. This difference is a consequence of the linearization process and the use of the phase jump as a validation event. Nevertheless, this difference does not take away from the use of the linearized model as it accurately reflects the dynamic behaviour of the system.

3.2 Small signal stability analysis

Using the validated linearized model, a parametric sensitivity is conducted to assess the system's stability when the grid's impedance is varied. While the SCR definition is not as straightforward in this setup, the grid's impedance is used as an accurate proxy for the grid's strength. The logic behind varying the grid's impedance remains equivalent to varying the SCR, especially considering the low value of the overhead lines' impedance.

The system displays high sensitivity to the grid's impedance. A higher L_g leads to a lower system's damping. The system becomes small-signal unstable for $L_g > 1\,p.u$. The same stability limit is found by simulating the non-linear model.

To better understand the mechanisms underlying the observed instability in figure 6, the eventually unstable eigenvalue is identified and its participation factors are studied. The results, shown in figure 7, describe the participation factors of all the state variables contributing to this eigenvalue, sorted by subsystem. It is observed that both converters highly contribute to the eigenvalue with the same control-related state variables. In fact, the three sets of state variables contributing the most are, in decreasing order: the PLL, the filtered inputs and the voltage regulation state variables.

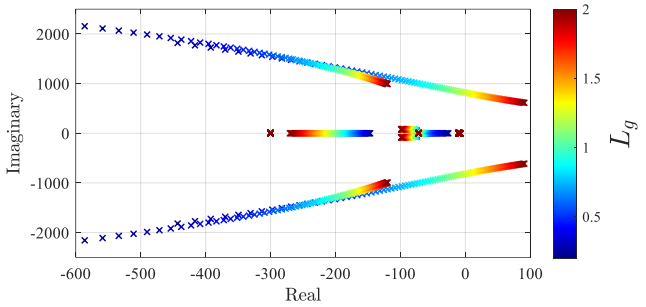

Fig.6 Parametric sensitivity to the grid's impedance

The voltage regulation state variables reflect the interactions between the two converters as their PCCs are electrically close with the OHL impedance being relatively small. Therefore, the voltage control loops are coupled through the interaction of the PCCs voltages. The filtered inputs are the state variables representing the inputs rotated by the PLL to the control reference frame. Their contribution to the eigenvalue here is effectively another manifestation of the PLL-related interactions. This phenomenon has been also observed by an impedance-based model, where it has been shown that the transformation in the park frame used for the voltages' and currents' input directly leads to a q-axis negative resistance, thus reducing the system's damping and stability margin [16]. Last, the PLL state variables' contribution confirms an expected interaction phenomenon that has been already reported in the literature, albeit using simplified models [17].

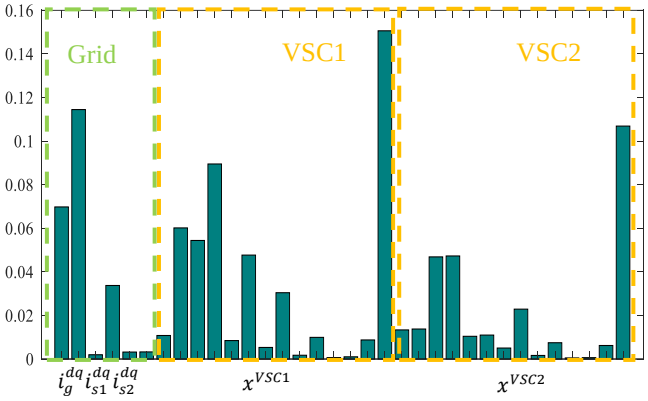

Fig.7 Participation factors of the identified eigenvalue

As it can be seen, the proposed setup has shown the true dynamic stability limit of the GFL controls without violating the physical limits of the converters' apparent and reactive powers. Furthermore, the setup has shown further instability mechanisms, such as the PLL-related interactions. Such insight allows for a better understanding of the real system's instability issues, unlike the Thévenin equivalent, as a high grid impedance is often correlated with long transmission distances, use of cables and proximity to other power-electronics interfaced sources. These findings also provide hints to potential improvements to the GFL control.

3 Improved GFL control

Using the insights provided by the proposed setup. Two improvements are identified to extend the stability of the GFL control. The improved control is shown in green and red in figure 8.

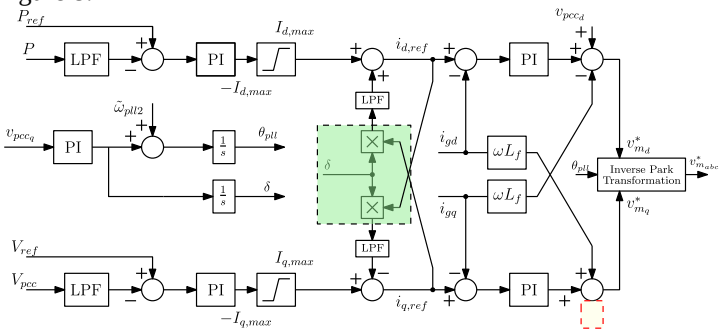

Fig. 8 Improved GFL control structure

First, the participation factors analysis shows a disproportionate contribution of the q-axis voltages compared to their d-axis counterparts. This phenomenon might be traced to the use of the q-axis voltage by the PLL for synchronization and for generating the control reference frame, this state variable is also used by the voltage regulation loop and by the current loop for the feedforward action. This can explain intuitively why it is more likely for the q-axis voltage to contribute more to the interaction phenomena and why it is more likely the root of the interaction phenomena. This is also in coherence with previously reported q-axis interactions [4], [18]. It is then possible to consider the reduction of the q-axis

use as a way to improve the stability of the control. It is impossible to discard $v_{pcc}^{q,ctrl}$ from the PLL as it is necessary for the synchronization of the control. The two remaining degrees of freedom are then the use of $v_{pcc}^{q,ctrl}$ for the voltage regulation or the voltage feedforward. The choice made in this work is discarding the use of $v_{pcc}^{q,ctrl}$ for the voltage feedforward, as shown in figure 8. The justification is twofold; the voltage regulation controls the norm of the voltage and the static error should account for the norm of the full voltage however small the q-axis contribution is. Meanwhile, the current control can reject the small disturbances around the null $v_{pcc}^{q,ctrl}$ steady state value using the integrator of the q-current PI controller.

A second improvement is inspired by the PLL-induced instabilities, as observed by the contributions of the filtered inputs rotated to the control reference frame. An impedance-based model has identified a simple way to compensate this destabilizing effect of the PLL by proposing an impedance reshaping method [19]. This method is further improved by considering a secondary PLL to insure the control's stability for frequency-variable conditions [16]. The double-PLL Impedance reshaping method is adopted in the present work.

The state space linearized model of the proposed control is built and validated in time domain using the proposed 2-VSC setup. The linearized model is then used to assess the sensitivity of the proposed control to the grid impedance variation. The results are shown in figure 9.

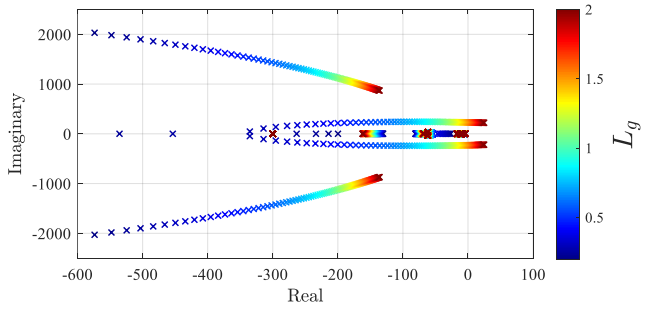

Fig. 9 Parametric sensitivity to the grid's impedance

While the system still displays high sensitivity to the grid's impedance, two improvements are significantly noticeable: first, the stability limit is improved by more than 40%, with the stability limit increasing from $L_g > 0{,}95\ p.u$ to $L_g > 1{,}42\ p.u$. This result has also been validated by simulating the non-linear model and verifying it shares the same stability limit. The second improvement is that the pair of eigenvalues that become unstable display higher damping, practically tripled around the critical stability limit. This means that the system can be operated close to its stability limit while maintaining acceptable damping.

For more insight on the impact of the proposed improvements, the participation factors of the eventually unstable are analysed. The results, as shown in figure 10, describe the participation factors of all the state variables contributing to this eigenvalue, sorted by subsystem. It is observed that both converters highly contribute to the eigenvalue with the same control-related state variables. The voltage regulation-related state variables contribute identically as before, and the PLL-related state variables are still the major contributors to the eigenvalue. Both results are logical and expected as the circuit parameters have not changed and the two converters remain electrically close.

More importantly, it is clear that the proposed improvements fulfil their intended goals: the filtered inputs-related state variables contribution, as well as the dissymmetry between the d-axis and q-axis state variables are drastically reduced.

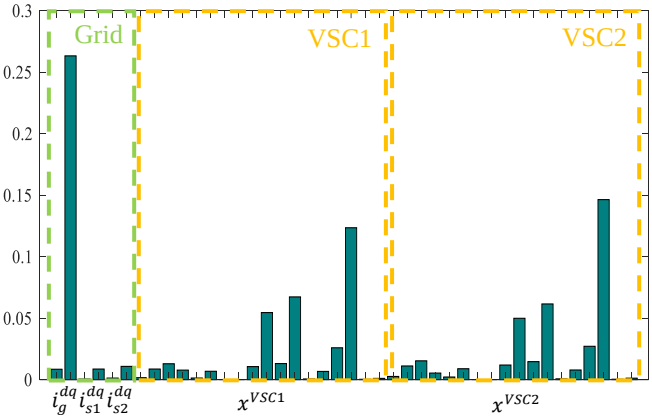

Figure 10 Participation factors of the identified eigenvalue

4 Conclusion and Perspectives

The present work has shown the limits of the common stability studies of Grid following control using the Thévenin equivalent. By analysing the controls' stability in a proposed 2-VSC system, it is shown that the stability analysis can be extended without reaching the static limit. A state-space linearized model is built and validated in time-domain. It is then used to show the control's sensitivity to the grid's impedance. The analysis of the participation factors offers insight into the instability mechanisms and the potential approaches to improve the controls' stability. Two improvements are proposed and tested. The improvements are shown to significantly improve the stability of the system and reduce the interactions among the converters.

Moving forward, these findings can be consolidated by building a parallel impedance-based model. This model will serve to first show the equivalence between both linearized models and to showcase the interaction phenomena differently, potentially leading to further improvements. The scalability of the impedance model can then be used to extend the findings to bigger, more complex systems.

5 References

[1] European Commission, "A European Green Deal." 2020.

[2] ENTSO-E, "Stability Management in Power Electronics Dominated Systems: A Prerequisite to the Success of the Energy Transition." Jun. 2022.

[3] J. Z. Zhou, H. Ding, S. Fan, Y. Zhang, and A. M. Gole, "Impact of Short-Circuit Ratio and Phase-Locked-Loop

Parameters on the Small-Signal Behavior of a VSC-HVDC Converter," *IEEE Trans. Power Deliv.*, vol. 29, no. 5, pp. 2287–2296, Oct. 2014, doi: 10.1109/TPWRD.2014.2330518.

[4] B. Wen, D. Boroyevich, R. Burgos, P. Mattavelli, and Z. Shen, "Analysis of D-Q Small-Signal Impedance of Grid-Tied Inverters," *IEEE Trans. Power Electron.*, vol. 31, no. 1, pp. 675–687, Jan. 2016, doi: 10.1109/TPEL.2015.2398192.

[5] M. F. M. Arani and Y. A.-R. I. Mohamed, "Analysis and Performance Enhancement of Vector-Controlled VSC in HVDC Links Connected to Very Weak Grids," *IEEE Trans. Power Syst.*, vol. 32, no. 1, pp. 684–693, Jan. 2017, doi: 10.1109/TPWRS.2016.2540959.

[6] J. F. Morris, K. H. Ahmed, and A. Egea-Àlvarez, "Analysis of Controller Bandwidth Interactions for Vector-Controlled VSC Connected to Very Weak AC Grids," *IEEE J. Emerg. Sel. Top. Power Electron.*, vol. 9, no. 6, pp. 7343–7354, Dec. 2021, doi: 10.1109/JESTPE.2020.3031203.

[7] W. Wang *et al.*, "Instability of PLL-Synchronized Converter-Based Generators in Low Short-Circuit Systems and the Limitations of Positive Sequence Modeling," in *2018 North American Power Symposium (NAPS)*, Sep. 2018, pp. 1–6. doi: 10.1109/NAPS.2018.8600590.

[8] L. Huang, C. Wu, D. Zhou, and F. Blaabjerg, "Comparison of Three Small-Signal Stability Analysis Methods for Grid-Following Inverter," in *2021 International Aegean Conference on Electrical Machines and Power Electronics (ACEMP) & 2021 International Conference on Optimization of Electrical and Electronic Equipment (OPTIM)*, Brasov, Romania, Sep. 2021, pp. 34–41. doi: 10.1109/OPTIM-ACEMP50812.2021.9590036.

[9] O. Gomis-Bellmunt, J. Song, M. Cheah-Mane, and E. Prieto-Araujo, "Steady-state impedance mapping in grids with power electronics: What is grid strength in modern power systems?," *Int. J. Electr. Power Energy Syst.*, vol. 136, p. 107635, Mar. 2022, doi: 10.1016/j.ijepes.2021.107635.

[10] R. Rosso, G. Buticchi, M. Liserre, Z. Zou, and S. Engelken, "Stability analysis of synchronization of parallel power converters," in *IECON 2017 - 43rd Annual Conference of the IEEE Industrial Electronics Society*, Oct. 2017, pp. 440–445. doi: 10.1109/IECON.2017.8216078.

[11] R. Rosso, S. Engelken, and M. Liserre, "Robust Stability Investigation of the Interactions Among Grid-Forming and Grid-Following Converters," *IEEE J. Emerg. Sel. Top. Power Electron.*, vol. 8, no. 2, pp. 991–1003, Jun. 2020, doi: 10.1109/JESTPE.2019.2951091.

[12] X. Wang, M. G. Taul, H. Wu, Y. Liao, F. Blaabjerg, and L. Harnefors, "Grid-Synchronization Stability of Converter-Based Resources—An Overview," *IEEE Open J. Ind. Appl.*, vol. 1, pp. 115–134, 2020, doi: 10.1109/OJIA.2020.3020392.

[13] L. Coronado *et al.*, "INELFE: main description and operational experience over three years in service," in *2019 AEIT HVDC International Conference (AEIT HVDC)*, May 2019, pp. 1–6. doi: 10.1109/AEIT-HVDC.2019.8740447.

[14] R. Teodorescu, M. Liserre, and P. Rodríguez, *Grid converters for photovoltaic and wind power systems*. [Piscataway, N.J.] : Chichester, West Sussex ; Hoboken, N.J: IEEE ; Wiley, 2011.

[15] Y. Li, S. Yang, K. Wang, and D. Zeng, "Research on PI controller tuning for VSC-HVDC system," in *2011 International Conference on Advanced Power System Automation and Protection*, Oct. 2011, vol. 1, pp. 261–264. doi: 10.1109/APAP.2011.6180414.

[16] L. Huang, C. Wu, D. Zhou, and F. Blaabjerg, "A Double-PLLs-Based Impedance Reshaping Method for Extending Stability Range of Grid-Following Inverter Under Weak Grid," *IEEE Trans. Power Electron.*, vol. 37, no. 4, pp. 4091–4104, Apr. 2022, doi: 10.1109/TPEL.2021.3127644.

[17] R. Rosso, M. Andresen, S. Engelken, and M. Liserre, "Analysis of the Interaction Among Power Converters Through Their Synchronization Mechanism," *IEEE Trans. Power Electron.*, vol. 34, no. 12, pp. 12321–12332, Dec. 2019, doi: 10.1109/TPEL.2019.2905355.

[18] Y. Liao, X. Wang, and F. Blaabjerg, "Passivity-Based Analysis and Design of Linear Voltage Controllers For Voltage-Source Converters," *IEEE Open J. Ind. Electron. Soc.*, vol. 1, pp. 114–126, 2020, doi: 10.1109/OJIES.2020.3001406.

[19] L. Huang, C. Wu, D. Zhou, and F. Blaabjerg, "A Simple Impedance Reshaping Method for Stability Enhancement of Grid-Following Inverter Under Weak Grid," in *2021 IEEE 12th International Symposium on Power Electronics for Distributed Generation Systems (PEDG)*, Jun. 2021, pp. 1–6. doi: 10.1109/PEDG51384.2021.9494181.